

EXPERIMENTAL INVESTIGATION OF SAIL AERODYNAMIC BEHAVIOR IN DYNAMIC CONDITIONS

Fabio Fossati

Politecnico di Milano – Department of Mechanics

Sara Muggiasca

Politecnico di Milano – Department of Mechanics

Manuscript received March 30, 2010; revision received July 30, 2010; accepted August 24, 2010.

Abstract: The aerodynamic behavior of a 48' yacht rig 3D scale model was characterized by means of wind tunnel tests. The experimental program, performed in the Politecnico di Milano Twisted Flow Wind Tunnel, allowed the aerodynamic forces to be characterized using forced motion tests and the aeroelastic behavior of the sail plan to be studied. Preliminary results are presented with reference to the typical encounter frequency range and typical pitch amplitudes corresponding to best yacht Velocity Made Good (VMG) condition for different true wind speeds and related sea states. A new representation of the aeroelastic effects is proposed in the form of aerodynamic hysteresis loops, obtained by plotting the sail plan aerodynamic coefficients against instantaneous apparent wind angle, varied using a harmonic law combining wind tunnel constant wind speed with sail plan center of effort velocity induced by yacht pitch motion. A "sail plan reduced velocity" concept is defined, and experimental results show that this reduced velocity play a fundamental role in sail plan aerodynamics. Finally, an estimate of the aerodynamic added mass effects is provided based on the comparison between the measured pitch moment during the "wind off" tests and the experimental test rig pitch moment of inertia.

Keywords: aerodynamics, experimental methods, hydrodynamics, model testing, motions, performance assessment, performance prediction, rigs, sails.

NOMENCLATURE

β_{AW}	Apparent wind angle
β_{din}	Dynamic apparent wind angle
β_{eff}	Effective angle
C	Chord length
C_D	Drag coefficient
C_L	Lift coefficient
C_x	Driving force coefficient
C_y	Heeling force coefficient
D	Drag force
f	Oscillation frequency
f_R	Reduced frequency
F_x	Driving force
F_y	Heeling force
g	Acceleration of gravity
H_{xi}	Yacht motion transfer function
I	Mass moment of inertia

I^*	Total system inertia
J_{added}	Added moment of inertia
L	Lift force
λ	Wavelength
μ	Heading angle
ω	Wave frequency
ω_e	Encounter frequency
ρ	Air density
S	Sail area
S_{ζ}	Sea waves energy spectrum
S_{xi}	Yacht motion energy spectrum
T_e	Encounter period
ϑ	Pitch angle
$\dot{\vartheta}$	Pitch angle velocity
U	Yacht speed
V	Flow velocity
V_{eff}	Effective wind speed
V_R	Reduced velocity
V_{ris}	Dynamic resultant wind speed
Z_{ceh}	Centre on effort height

INTRODUCTION

One of the most challenging tasks in yacht design modelling and simulation is the development of methods and tools for the analysis of yacht behaviour in a realistic environment. One particularly difficult task is developing time domain approaches that simulate yacht motion, including manoeuvring and course-keeping, when under sail in a seaway. To overcome these difficulties, modelling must move from Velocity Prediction Programs (VPP) to Performance Prediction Programs (PPP).

Traditionally, a VPP solves static yacht equilibrium equations by assuming that the yacht is sailing on a straight course at a constant speed with no accelerations. Because of this, current sailing yacht aerodynamic force models are based on steady-state assumptions.

Sail forces acting on a sailing yacht are expressed in terms of sail plan aerodynamic coefficients as functions of apparent wind angle generally available from wind tunnel tests or Computational Fluid Dynamics (CFD) results at different apparent wind angles. To reproduce the effects of sail trim, a number of de-powering models have been introduced in steady-state aerodynamic models (Kerwin, 1978; Hansen, 2006; Fossati, 2008).

However, steady-state conditions are mere abstractions. In real sailing conditions, the wind varies in direction and strength, and wave systems disturb and act upon the yacht's motion. Accelerations on the boat's degrees of freedom are produced because of wind and wave variations and changes in rudder angle. In these conditions, time appears explicitly in the equations governing yacht motion. As a result, these equations become a system of differential equations (generally non-linear) that must be integrated in the time domain.

Several models and computer codes, called Dynamic Velocity Prediction Programs (DVPPs), have been developed (Keuning, 2007; Masuyama, 1993; Masuyama, 2005; Richardt, 2005) to account for unsteady conditions on sailboat dynamics. These programs are based on Newton's law and require the hydrodynamic and aerodynamic forces acting

on the sailboat to create models. The dynamic effects of hydrodynamic forces acting on the yacht hull and appendages have been heavily researched; however, the dynamic effects of aerodynamic forces have not.

Most authors use the steady-state approach based on force coefficients empirically derived or measured from wind tunnel experiments as a function of the apparent wind angle. Other authors (Keuning, 2005; Richardt et al, 2005; Harris, 2002; Contento, 2006) include the velocities induced by the roll and the yaw motions into the apparent wind angle and apparent wind speed expressions using the Quasi Steady Theory (QST) approach.

Masuyama (1995) introduced a completely different approach based on neural network schematization. This approach represents a very useful option even if it does not provide any insight into the physics of the sail in unsteady flow.

Gerhardt (2008) used unsteady potential flow theory to predict the pressure distribution on a two dimensional “slice” of a mainsail undergoing harmonic oscillations perpendicular to and along the direction of the incident flow. Then he compared the theoretical predictions to actual wind tunnel measurements on an oscillating 2D rigid mainsail slice model. He concluded that aerodynamic performance can only be predicted using an unsteady aerodynamic model.

To the authors’ knowledge, the first attempt to develop specific experiments providing an insight into the physics of unsteady sail aerodynamics are described by Fossati (2009). The present work, which is a revision of Fossati (2009), is a first step in investigating sail plan aerodynamics in unsteady conditions, particularly wave-induced yacht pitch motion frequency and amplitude effects on sail forces.

In the present study, the unsteady conditions were investigated in the Politecnico di Milano Twisted Flow Wind Tunnel using a carbon-fiber manufactured rig scale model of a 48’ cruiser-racer sloop. The model was tested using forced motion dynamic tests within the typical encounter frequency and pitch amplitude ranges, both of which were chosen to correspond with the best yacht VMG conditions for different true wind speeds (TWS) and relevant sea states.

The sail plan rigid model was designed using sail flying shapes available from previous tests carried out with the same sail plan model.

As an extension of Fossati’s (2009) work, an estimate of the aerodynamic added mass effects is provided based on the comparison between the measured pitch moment during the “wind off” tests and the experimental test rig pitch moment of inertia.

WIND TUNNEL EXPERIMENTS DESIGN

To assess the unsteady effects in sail aerodynamics, we must consider a yacht pitching in waves (Figure 1). Both the apparent wind speed (V_{AW}) and apparent wind angle (β_{AW}) corresponding to the steady-state conditions change because of pitch-induced velocity. This results in a new apparent wind speed (V_{ris}) and a new apparent wind angle (β_{din}) (Figure 2). Both change over time and depend on the particular pitch rate considered.

The problem is similar with other motions. However, to keep the experiment as simple as possible, only yacht pitch motion was considered for this study.

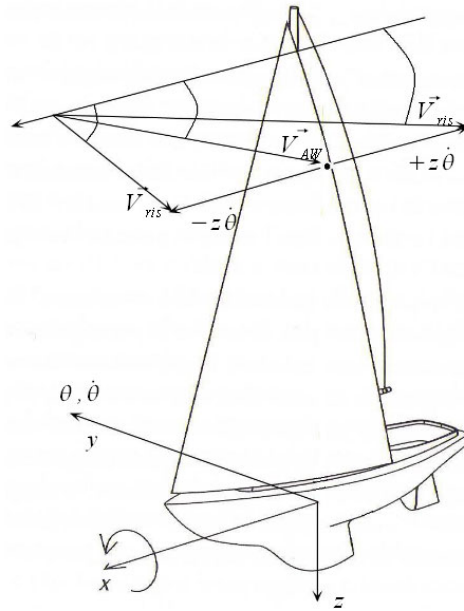


Figure 1. Wind triangle resulting from yacht pitch motion.

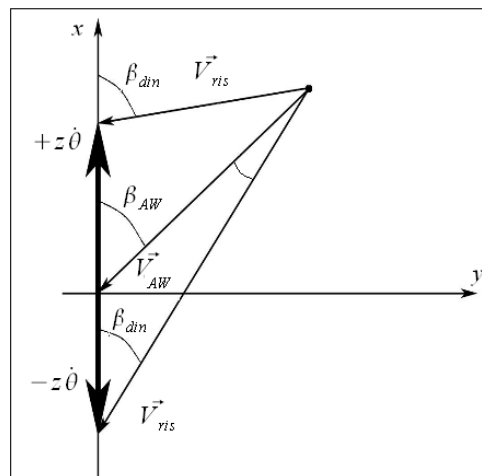


Figure 2. Dynamic effects on wind triangle.

Aerodynamic similarity between the model and full-scale observations must be achieved during wind tunnel experimental tests in order to investigate wave-induced yacht pitch motion frequency and amplitude effects on sail forces. Studies on oscillating airfoils in other fields, particularly the aeronautical sector (Glauert, 1948; Schlichting, 1979; Molyneux, 1956; Milgram, 1971; Dickinson, 1993; Lee, 2004; Moss, 1971), have shown that reduced velocity (V_R) and its reciprocal, reduced frequency (f_R), are the parameters governing the mechanism of lift prediction. V_R and f_R are defined as follows:

$$\begin{aligned}V_R &= \frac{V}{fC} = \frac{VT}{C} \\f_R &= \frac{fC}{V} = \frac{C}{VT}\end{aligned}\tag{1}$$

where:

- V = flow velocity
- C = airfoil chord
- f = airfoil oscillation frequency
- T = oscillation period (1/f)

Since the reduced frequency is directly proportional to the airfoil oscillation frequency, it is a parameter that expresses the speed at which the angle of incidence varies.

It is also interesting to observe that the reduced velocity (equation 1) also shows the relationship between the airfoil oscillation period and the time (C/V) taken by a fluid particle to cover the length of the chord, or the time needed to cross the area intersected by the wing section. Reduced frequency describes the converse relation.

The shorter the time needed to cross the airfoil region relative to the time needed to complete an oscillation (the period T), that is for high values of reduced velocity or low values of reduced frequency, the more we can consider the conditions of the fluid-airfoil interactions to be static. When this happens, the formulae discussed earlier for calculating the fluid forces become more valid. On the other hand, the smaller the reduced velocity (or the greater the reduced frequency) the more the interaction conditions will differ from those of the static state, and specific information on the forces developed in dynamic conditions is needed.

From previous work in wind engineering (Theodorsen, 1949; Caracoglia, 2003; Jones, 1996), a reduced frequency higher than 0.05 indicates that the contribution of added mass and unsteady vortex shedding to the overall lift is too large to neglect so the problem must be considered to be unsteady.

Based on equation (1), if the wind speed in a wind tunnel experiment is the same as the wind speed in the full scale boat, a 1:10 scale model must be oscillated 10 times faster than the full-scale boat. Because of this, designing wind tunnel tests with the same reduced frequency range as the full-scale model is difficult. To reduce the scale model inertia, a simplified rig model consisting of only the rig and sails (without hull and deck details) was built.

If the model sails are not rigid, oscillating the scaled model at high frequencies can lead to changes in sail shape. These changes will affect the forces that are produced. To address this problem, a rigid carbon fiber manufactured rig 1:10 scale model of a 48' cruiser-racer sloop was produced for the wind tunnel experiments.

Since rigid sails cannot be trimmed, the sail plan rigid model was designed using sail flying shapes that correspond to maximum driving force trimming condition available from previous tests carried out with the same sail plan scale model.

Steady aerodynamic forces and three-dimensional sail shapes were previously measured in upwind conditions at different apparent wind angles and sail trim settings using the

traditional testing procedure in steady-state conditions (Fossati, 2006). The measured flying shapes were obtained in real time during the tests using a photogrammetry computer-based IR-camera system developed in-house (Fossati, 2008). For the present study, the system consisted of five cameras to simultaneously film the reflective targets placed on sails, and a computer equipped with custom-made acquisition and processing software (Figure 3).



Figure 3. Flying shape measurement system.

Highly reflective markers (8 mm in diameter) were glued to each sail at 8 horizontal sections, plus one on the top (Figure 4).

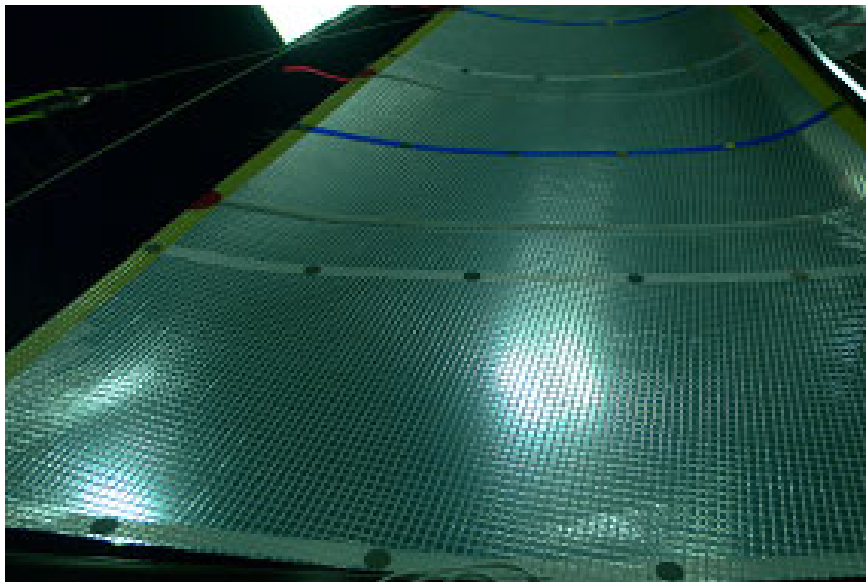


Figure 4. Reflective markers on the main.

The custom-made software performed real-time blob detection and stored the camera images on a hard disk. As a result of this routine a table with the 2D blob detected coordinates is available for post processing.

Cameras were calibrated beforehand using a custom-built calibration frame. After calibration the 3D marker point coordinates for each sail were obtained using a Direct Linear Transformation (DLT) algorithm, defining the marker positions with an uncertainty equal to 0.5 mm.

The 3D points array was used for surface modeling (Figure 5). Then, a computer-aided molding machine created the scale-model sail molds from the modeled surfaces (Figure 6).

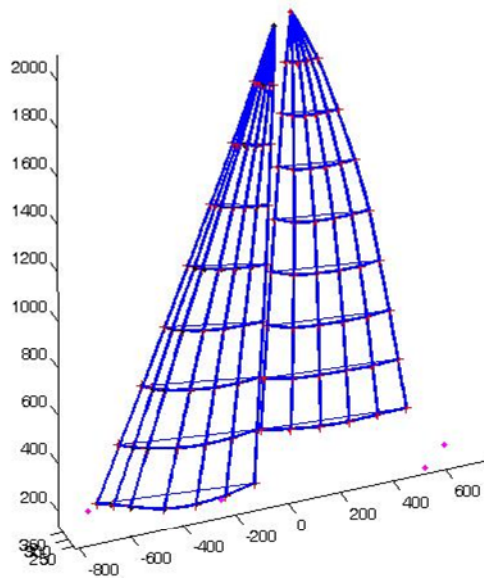


Figure 5. Flying shape surface modeling.



Figure 6. Carbon fiber mainsail model.

The dynamic wind tunnel test results presented below refer to sail flying shapes corresponding to sail trim that provides the maximum driving force achievable.

The yacht pitch amplitude and frequency range caused by the waves passing beneath it were estimated using the main yacht dimensions (Table 1) and the principal dimensions of the yacht model sail plan (Table 2).

Table 1. Main yacht dimensions.

LOA (m)	14.5
BMAX (m)	4.29
LWL (m)	12.89
DISPL (kg)	13000
SAIL AREA (m ²)	118

Table 2. Main scaled sail plan dimensions.

I	1970 mm
J	600 mm
P	1760 mm
E	568 mm

Prof. Keuning of Delft University of Technology provided the heave and pitch Response Amplitude Operator (RAO) for Model 455 from the Delft Systematic Yacht Hull Series (DSYHS). This model has similar characteristics to the present model. The RAO was obtained from towing tank tests both in upright and 20° heel conditions.

Figure 7 shows the pitch/wave slope RAO as a function of the LWL/wavelength ratio for the yacht.

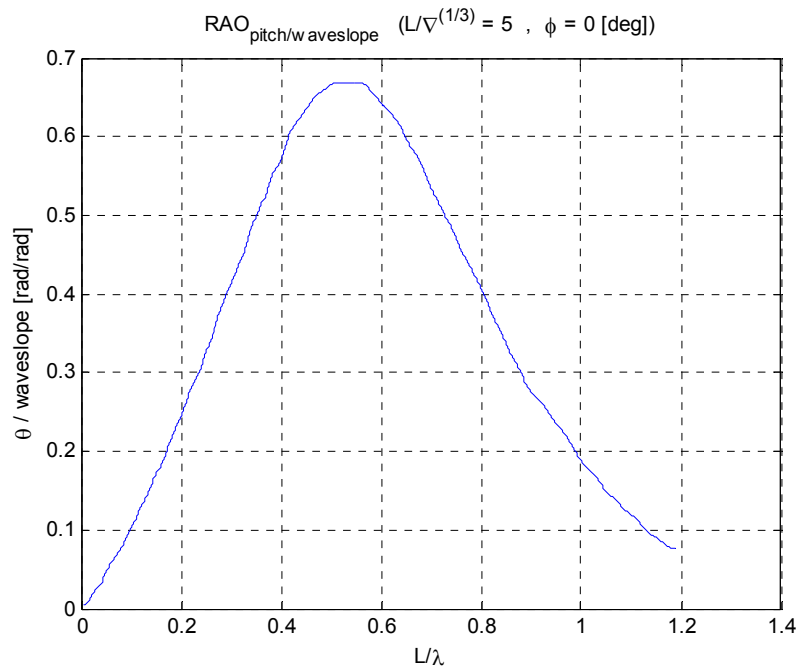


Figure 7. Pitch Response Amplitude Operator vs. L_{WL}/λ .

Using the well known linear wave theory relationship we can express the pitch angle amplitude RAO divided by the wave amplitude in terms of wave frequency (Figure 8).

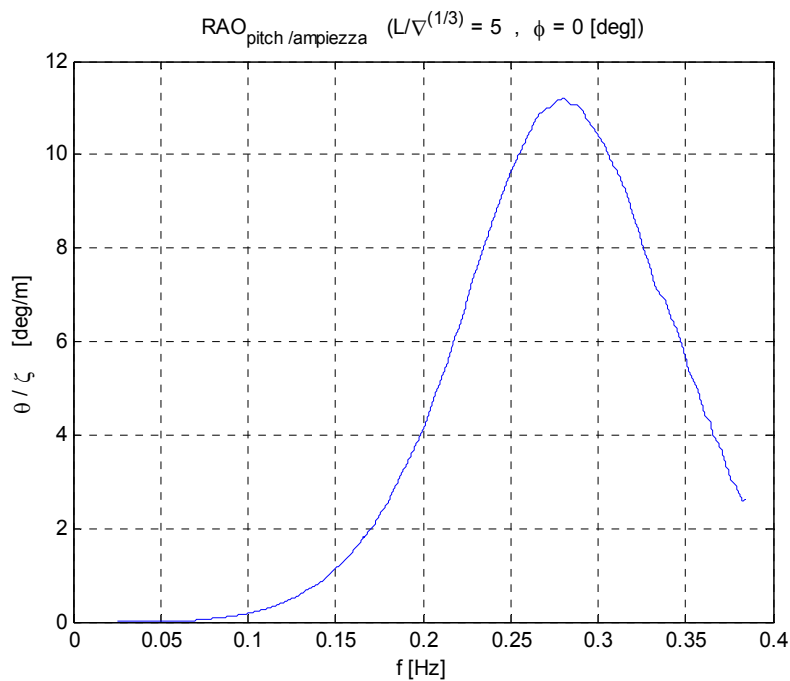


Figure 8. Pitch RAO vs. wave frequency.

The speed of the yacht must be taken into account when considering the pitch RAO because it affects the encounter frequency:

$$\omega_e = \omega - \omega^2 \frac{U}{g} \cos(180 - \mu) \left[\frac{\text{rad}}{\text{s}} \right] \quad (2)$$

where:

ω = wave frequency (rad/s)

ω_e = encounter frequency (rad/s)

U = yacht speed

g = acceleration of gravity

μ = heading angle

In order to estimate the full scale yacht encounter frequency range, performance predictions at different true wind speeds and true wind angles were obtained using the Offshore Racing Council International Velocity Prediction Program. The full scale yacht VMG and the corresponding apparent wind angle were evaluated for each TWS. Then, the full scale yacht encounter frequency range was calculated using the yacht velocities.

If the incoming wave direction is the same as the direction of the true wind, then the heading angle of equation (2) can be evaluated.

Figure 9 shows the pitch RAO as a function of the encounter frequency for the yacht. Each RAO curve corresponds to an upwind VMG obtained at each TWS considered in the VPP study.

The final step is to evaluate the pitch response in waves. Several formulas exist for expressing in analytical form the idealised wave energy spectra as a function of characteristic parameters such as the significant wave height ($H_{1/3}$) and the average period (T_0) of the spectrum.

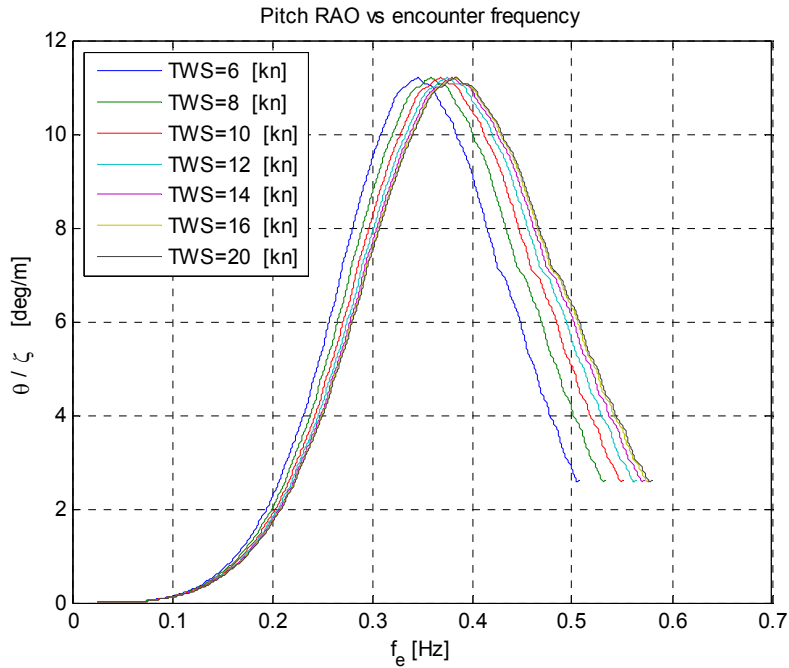


Figure 9. Pitch Response Amplitude operator vs. encounter wave frequency.

Different expressions are used for large fetch conditions (open sea) and coastal conditions (limited fetch). For the present study the Bretschneider energy spectrum, which is particularly suited for representing conditions in mid ocean, was used. This spectrum is expressed as

$$S_{\zeta}(\omega_n) = \frac{A}{\omega^5} \exp\left(\frac{-B}{\omega^4}\right) \quad \left(\frac{m^2}{rad/s}\right) \quad (3)$$

where:

$$A = 172.75 \frac{H^{1/3}}{T_0^4} \quad \left(\frac{m^2}{s^4}\right) \quad (4)$$

$$B = 172.75 \frac{691}{T_0^4} \quad (s^4)$$

In order to link wind intensity to significant wave height and the period of the spectrum, relationships relating to the North Atlantic (Claughton, 1988) were used (Figure 10).

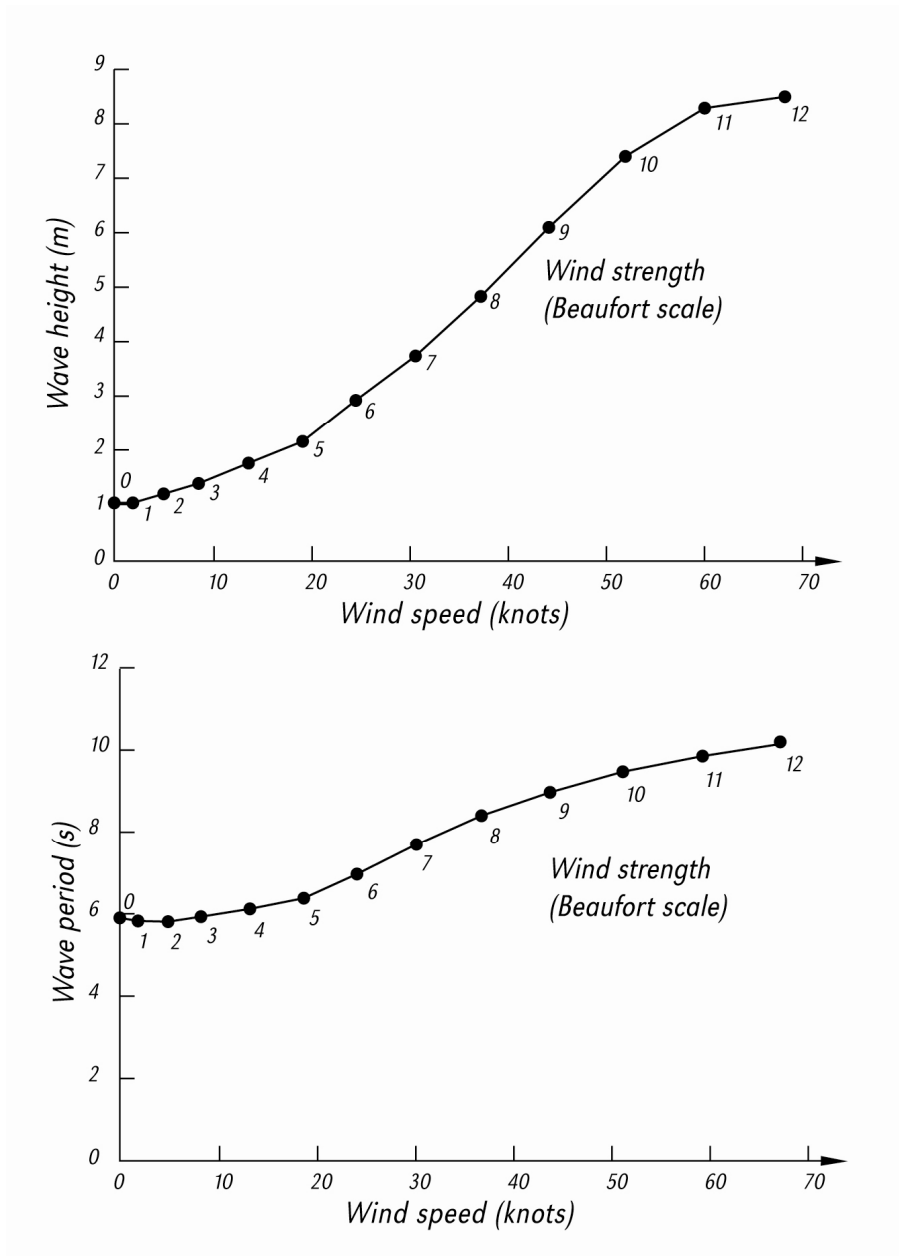


Figure 10. Wave significant height and wave period versus wind speed.

Figure 11 shows the Bretschneider energy spectrum for the wind intensities considered for the reference yacht performance prediction at full scale.

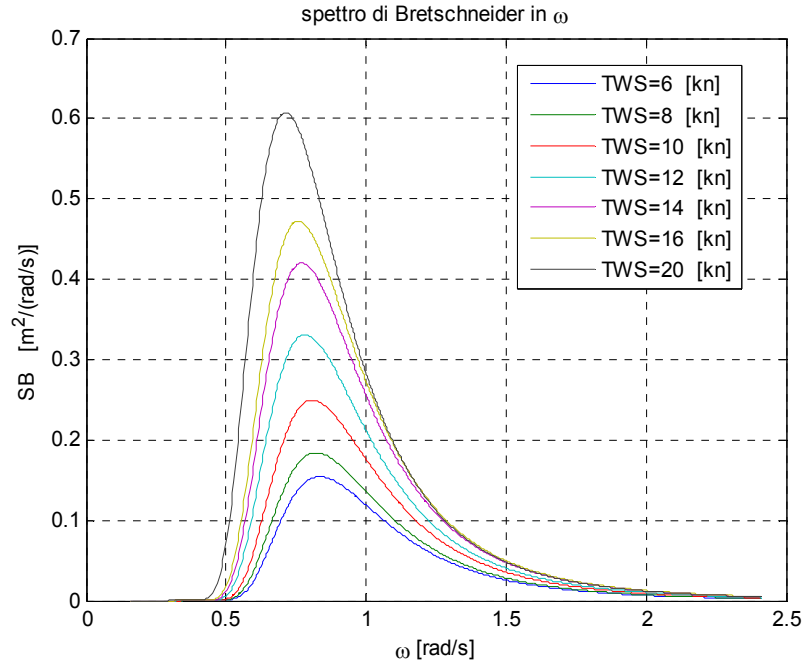


Figure 11. Bretschneider sea waves energy spectrum.

To calculate the yacht response in irregular waves characterized by a given wave energy spectrum, it can be shown that the motion energy spectrum in each degree of freedom is given by the product of the square of the motion transfer function (RAO) of each degree of freedom and the wave energy spectrum. The pitch response of the yacht over the whole frequency range can be calculated using equation (5).

$$S_{x_i}(\omega) = H_{x_i}^2(\omega)S_{\zeta}(\omega) \quad i = 1, 2, \dots, 6 \quad (5)$$

Figure 12 shows the pitch response spectrum versus encounter frequency for the full-scale yacht at different true wind strengths.

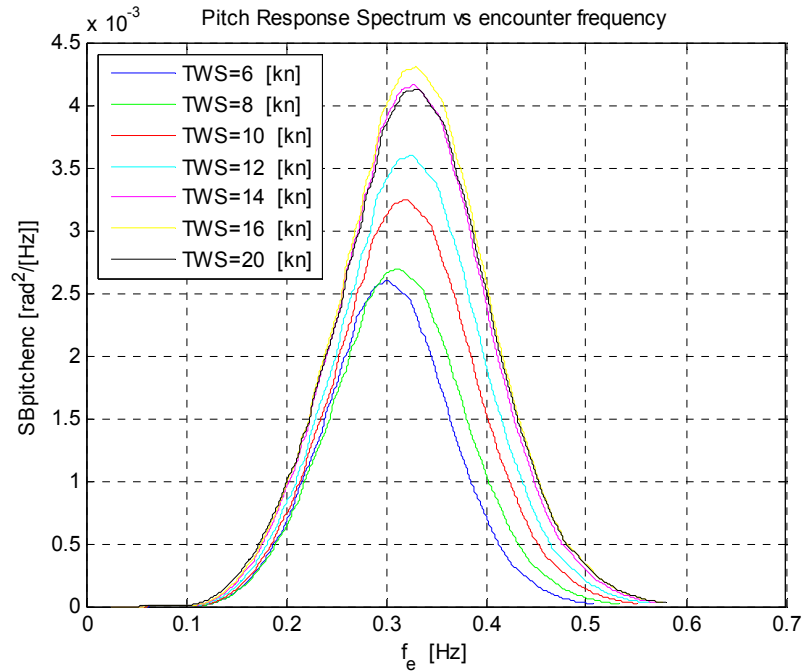


Figure 12. Pitch response spectrum vs. encounter frequency.

The resulting pitch response energy spectrum shows that the most significant yacht response is in the following frequency range:

$$0.07 < f_e < 0.55 \text{ [Hz]} \quad (6)$$

This can also be expressed as the following encounter period range:

$$1.8 < T_e < 14.3 \text{ [s]} \quad (7)$$

Yacht pitch time histories can be evaluated using the superimposition of harmonic components using random phases from the pitch response energy spectrum. Figure 13 shows a typical pitch time history for the 20 knot TWS in VMG conditions.

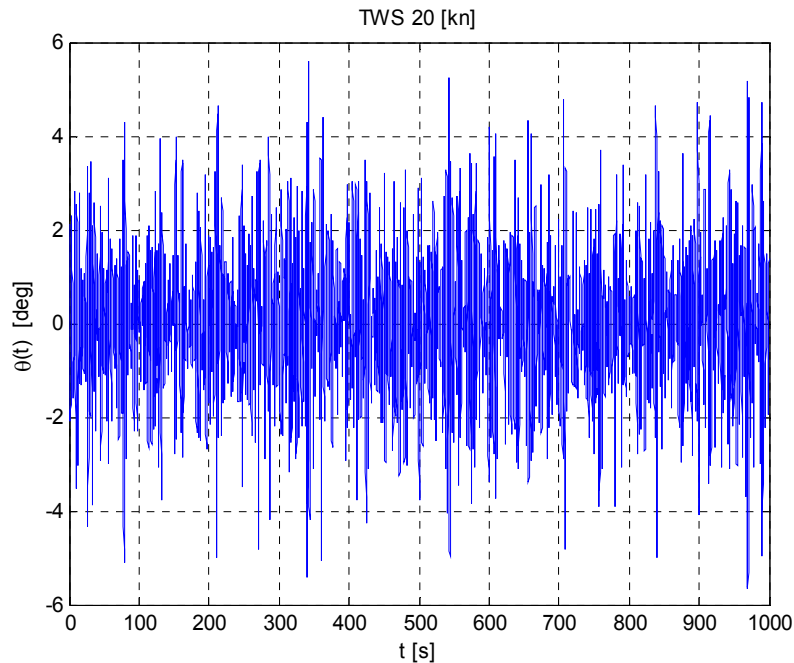


Figure 13. Sample of typical pitch time history at 20 knots TWS.

Typical full scale yacht pitch response amplitudes and frequency ranges have been evaluated in order to tune the fundamental parameters of the dynamic tests. As noted earlier, V_R and f_R must be the same between the model and full-scale to maintain aerodynamic similarity.

Performing forced oscillation tests of the yacht sail plan is different than forced oscillations of an airfoil. The influence of 3D effects and unsteady mainsail-jib interaction must be considered. However, when using the equation for f_R , it becomes unclear if a specific chord length is representative of the unsteady aerodynamics:

$$f_R = \frac{fC}{V} \quad (8)$$

To overcome this problem, the authors hypothesized that the sail plan chord evaluated at the center of effort (Z_{CEH}) could be used in equation (8), as shown in Figure 14.

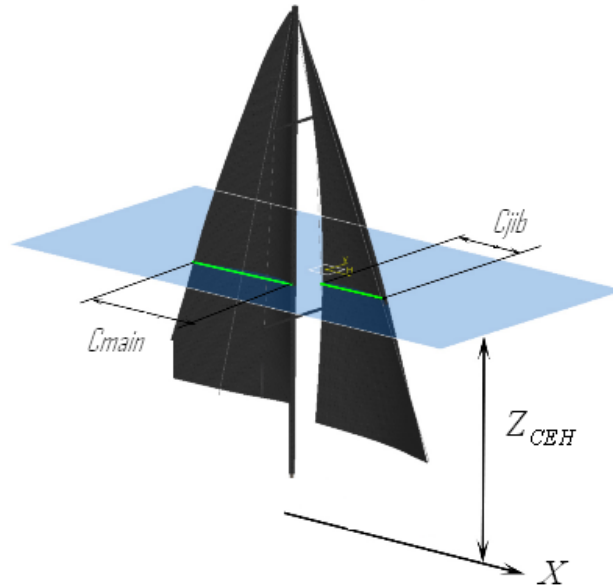


Figure 14. Sail plan chord length definition.

The full-scale chord length of the 48' cruiser racer used for this study was 5.7 m based on the Z_{CEH} from steady-state conditions using traditional wind tunnel tests. Using the TWS range considered in the VPP computations (6 knots – 20 knots) and the expected encounter frequency range from equation (6), the reduced frequency range is:

$$0.04 < f_R < 1.05 \quad (9)$$

The forced pitch frequency oscillation of the model was limited to 1.2 Hz because of the model's structural strength limits. To obtain a low V_R during the experiments, wind tunnel speed was reduced as much as possible without compromising the resolution of the dynamometer.

Because of these limitations, wind tunnel tests were performed in the following test wind speed range:

$$2 < V_{wind} < 4 \quad [m/s] \quad (10)$$

This resulted in the following V_R and f_R ranges:

$$\begin{aligned} 0.018 < f_R < 0.426 \\ 2.3 < V_R < 56 \end{aligned} \quad (11)$$

Tests were performed at forced pitch oscillation amplitudes within the following range to investigate the effects of pitch amplitude on sail aerodynamics.

$$2 < \vartheta < 10 \quad [deg] \quad (12)$$

In addition to matching the reduced velocity and frequency, Reynolds number should also be matched during the experiments. However, this is impossible to achieve using a scale model. First, increasing the wind tunnel velocity to increase the Reynolds number leads to an increase of the rig model oscillation frequency because of V_R constraints. As a result of inertia, structural problems arise on the model. Second, when experimenting with unsteady conditions, the V_R should be as low as possible. Reduced wind speed, however, results in an incorrect Reynolds number. To overcome these limitations, the leading edge boundary layers were tripped.

TEST RIG AND EXPERIMENTAL SET-UP

The scale model was connected to a dynamometric balance, and the balance was attached directly to a pitching device that delivers a purely harmonic motion allowing the rig to be pitched around the estimated yacht pitch axis (Figure 15). The yacht pitch axis was evaluated considering the shape of the yacht waterplane area in an upright condition and the relevant position of the transverse rotation axis.

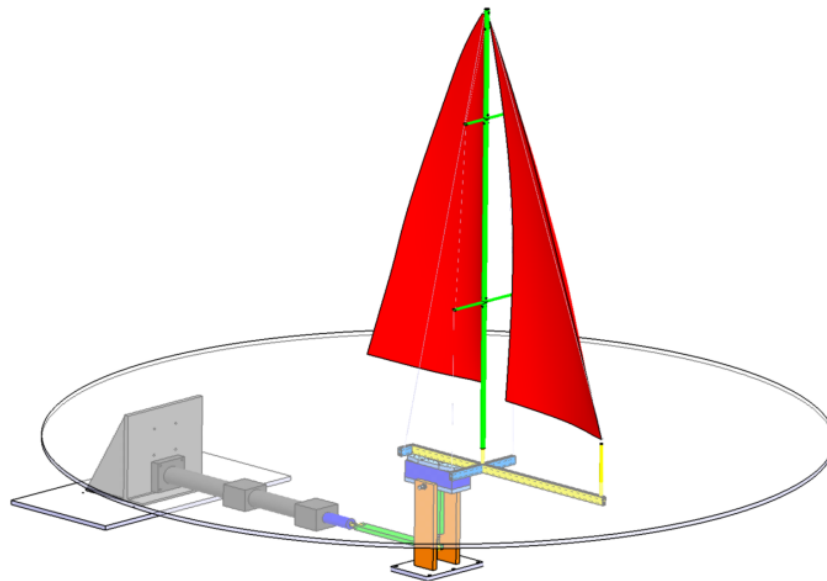


Figure 15. Pitching device and 3D sail plan model.

A computer-controlled servo-hydraulic actuator was used to drive the rig forced motion, allowing the pitch amplitude and frequency for the test to be chosen.

The dynamometric balance (Figure 16) has seven strain gauge channels that accurately measure the vertical, longitudinal, and lateral forces and the three moments around the three principal axes using a calibration matrix provided by the supplier.

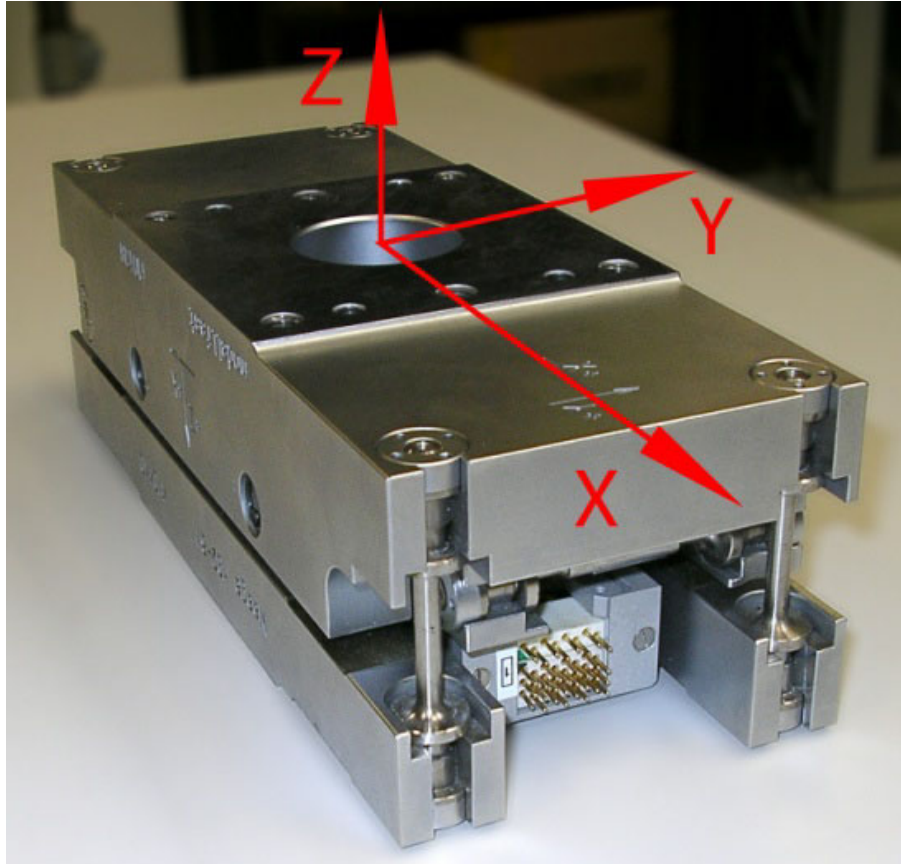


Figure 16. Dynamometric balance.

The calibration matrix was provided with reference to static conditions. To check the dynamometric balance dynamic response function, forced motion tests were carried out earlier with an electro-dynamic shaker (Figure 17). The results showed that no significant phase shift was introduced between the forces and displacements in the frequency range of interest.

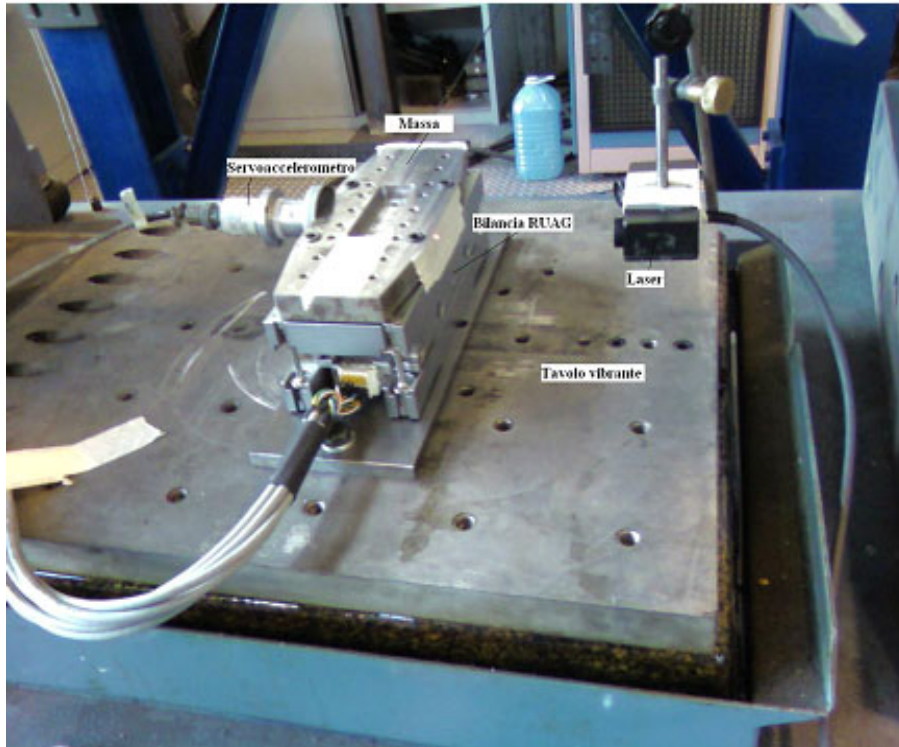


Figure 17. Dynamometric balance dynamic characterization.

A flat plate was placed at the foot of the test rig mast to reproduce free surface boundary conditions (Figure 15).

Figure 18 shows a detail of the test-rig/balance connection and the pitching device. A laser transducer measured the rig angular displacement during the forced motion tests when the model was linked to the hydraulic dynamic actuator.

Different pitch amplitudes and frequencies were combined to obtain different apparent wind speeds and apparent wind angle variations. This reproduced the full-scale forces acting on the sail plan by accounting for the pitch motion caused by sea waves.

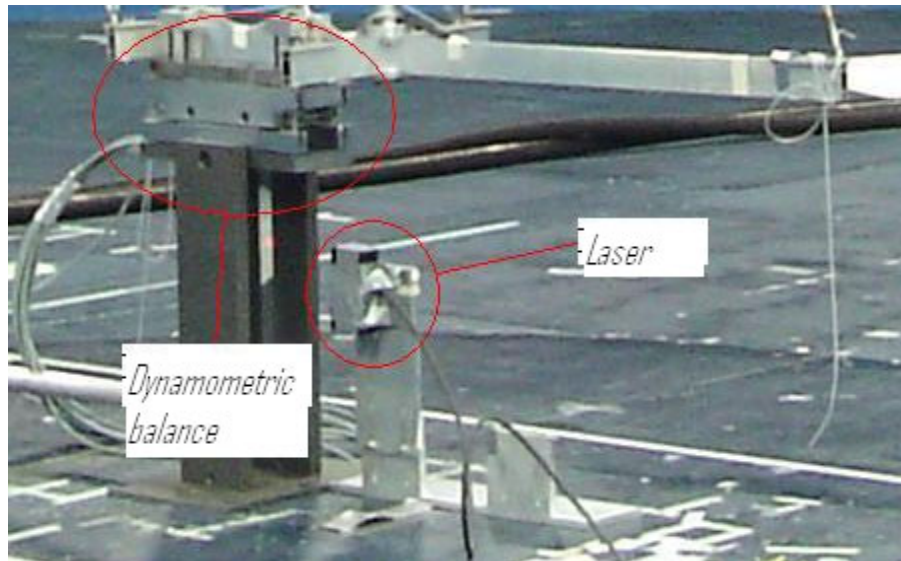


Figure 18. Dynamic test-rig details.

WIND TUNNEL TESTING PROCEDURE

Three types of tests were performed: steady-state tests, tests with the model oscillating at a fixed frequency with different pitch amplitude, and tests with the model oscillating at constant pitch amplitude with different motion frequencies.

The experiments were conducted and the aerodynamic forces and moments around the three principal axes were measured at wind speeds of 2 m/s, 3 m/s, and 4 m/s. These wind speeds represent the apparent wind speed of the yacht in steady conditions. They were measured at a reference height of 1 m to correspond to the full-scale height of 10 m.

During the steady-state tests the model was at rest with an apparent wind angle 22° based on the sail flying shapes used to create the model. The measured aerodynamic forces were compared with the results of previous steady-state tests using the scale model equipped with sail trimming devices in maximum drive condition (Figure 2).

The analog signals from the force measurement system were analog low-pass filtered and then digitally sampled and processed.

“Wind-off” tests were performed for each frequency and pitch amplitude combination to account for the inertia acting on the oscillating rig. The difference between “wind-on” and “wind-off” measurements was then used to evaluate the aerodynamic forces developed by the sail plan in dynamic conditions.

BASIC POSITIONS

The instantaneous center of effort height Z_{CEH} is fundamental for computing the chord length in the reduced velocity evaluation. Z_{CEH} was determined using the ratio between the aerodynamic heeling moment and heeling force (Figure 19). The wind triangle was then solved using the effective angle theory on a plane perpendicular to the mast (Jackson, 2001). The sail plan center of effort was used as the reference point for the instantaneous apparent wind speed and the instantaneous apparent wind angle.

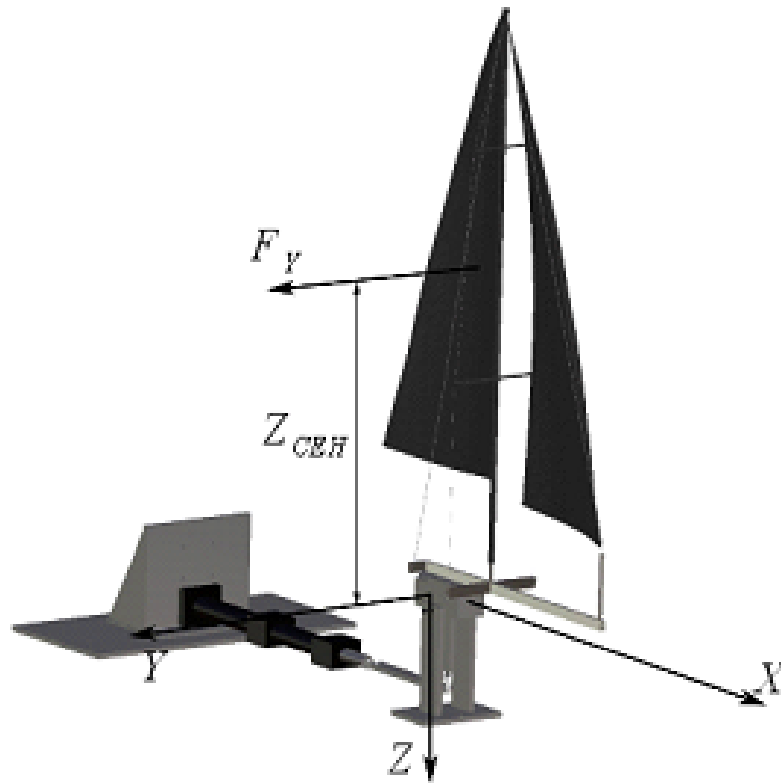


Figure 19. Instantaneous center of effort.

When a yacht is sailing with heel and pitch, the onset flow is no longer perpendicular to the leading edge of the sails. The resulting lift and drag become a function of both the apparent wind angle (β_{AW}) and the heel and pitch angles. To account for this, the effective angle concept was used.

The yacht model had no heel during the tests, so the flow component along the chord of the sails was influenced by the pitch angle. The effective angle β_{eff} is geometrically related to the apparent wind angle β_{AW} and to the pitch angle θ and can be calculated from:

$$\beta_{eff} = \tan^{-1} \left(\frac{\tan \beta_{AW}}{\cos \theta} \right) \quad (13)$$

Similarly the effective wind speed V_{eff} can be obtained from β_{AW} and θ as a fraction of the apparent wind speed V_{AW} (the wind tunnel reference speed) as:

$$V_{eff} = V_{AW} \sqrt{(\sin^2 \beta_{AW} + \cos^2 \beta_{AW} \cos \vartheta)} \quad (14)$$

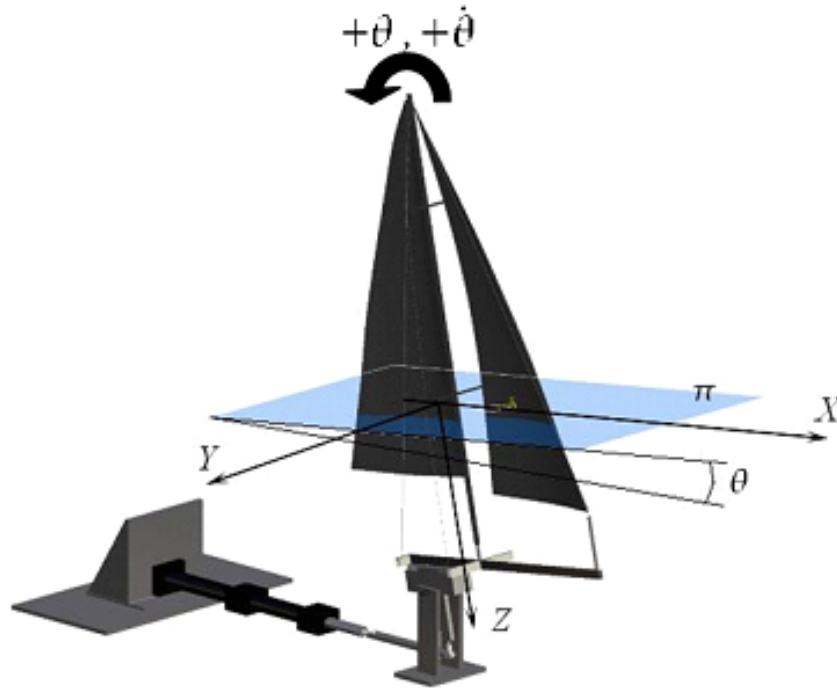


Figure 20. Reference plane π for the effective angle evaluation.

The combination of the dynamic velocity at the center of effort due to yacht pitch angular velocity (Figure 20) with the steady-state effective speed V_{eff} leads to the dynamic resultant wind speed V_{ris} and apparent wind angle β_{din} shown in Figure 21.

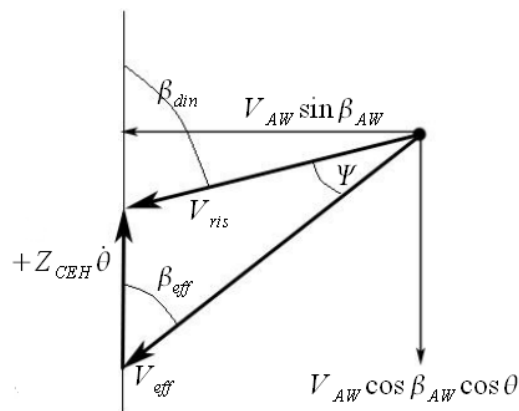


Figure 21. Effects of pitch motion on wind triangle.

In the present work dynamic lift and drag were evaluated on the π plane from the difference between “wind-on” and “wind-off” measured forces considering the direction of the apparent wind angle β_{din} . The aerodynamic coefficients were defined in dynamic conditions with reference to the dynamic resultant wind speed V_{ris} (Figure 22).

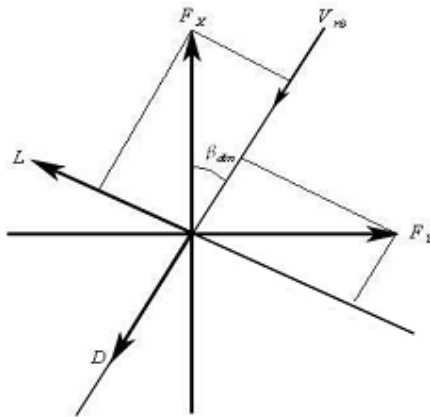


Figure 22. Sail plan lift and drag definition.

DATA PROCESSING

During the wind tunnel experiments all tests were performed with the rig model harmonically excited with different pitch amplitudes and different motion frequencies at different wind speeds. To account for inertial forces acting on the oscillating rig “wind-off” tests were performed corresponding to each chosen frequency and pitch amplitude combination. The difference between “wind-on” and “wind-off” measurements was then used to evaluate the aerodynamic forces developed by the sail plan in dynamic conditions.

In order to determine this difference a time history of digitalized signals from the force measurement system containing an exact number of periods was extracted, using the rig model pitch oscillation signal as a reference. For example, in the case with a harmonic pitch oscillation of 3.5° at an amplitude of 0.5 Hz, five periods of pitching oscillations were extracted from the longer record, then all other signals were referred to this reference pitch motion (Figure 23).

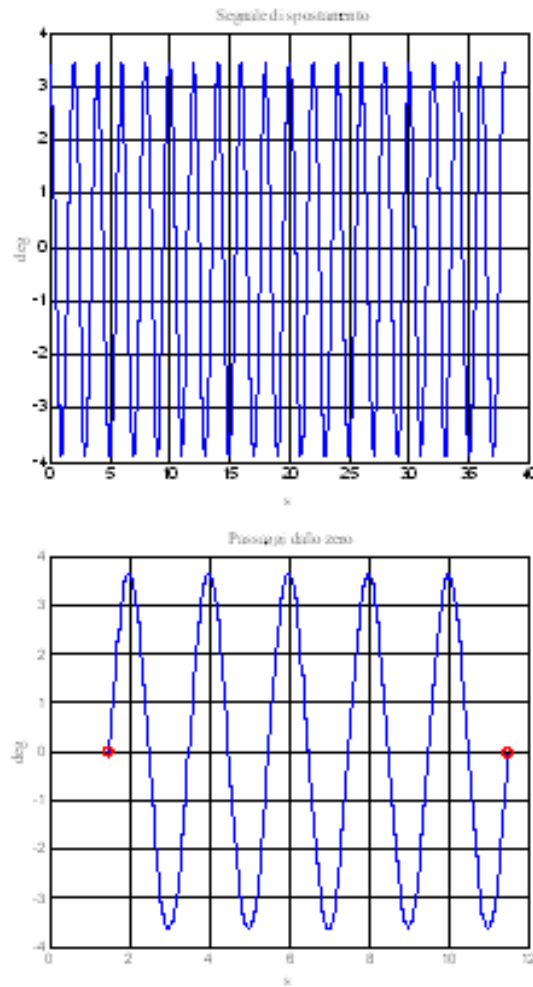


Figure 23. Rig model forced pitch motion reference signal.

Figure 24 refers to a dynamic test in steady-state conditions with an apparent wind angle of 22° and an apparent wind speed of 2.95 m/s. Figure 24a shows the corresponding time histories of the center of effort velocity \dot{z}_{CEH} induced from the pitch angular speed, while Figures 24b and 24c show respectively the dynamic resultant wind speed V_{ris} and the dynamic apparent wind angle β_{din} time histories evaluated at the centre of effort height, based on Figure 21.

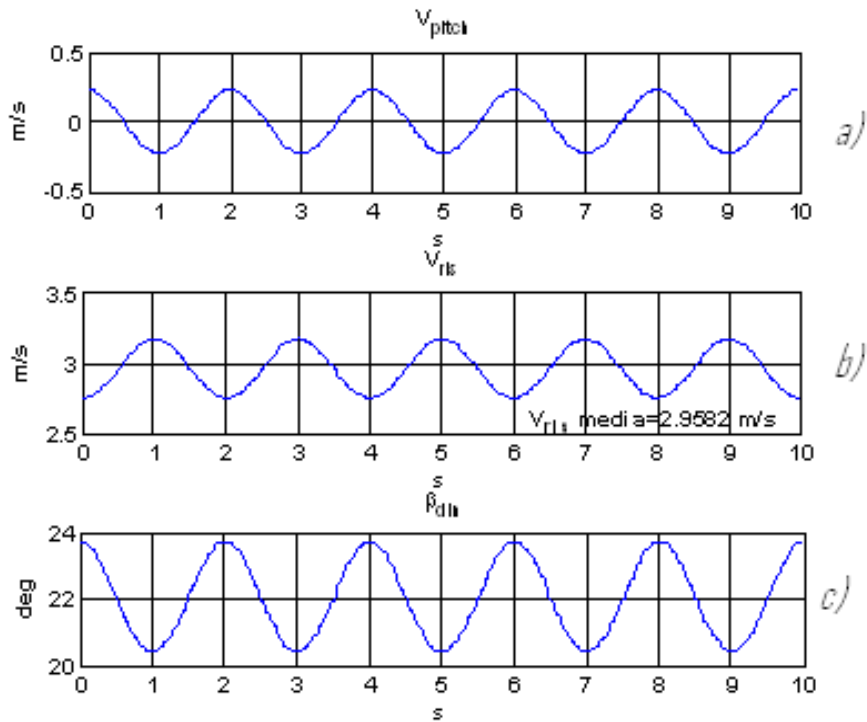


Figure 24. Time histories samples of: center of effort velocity induced by pitch angular speed (a), dynamic resultant wind speed (b), dynamic apparent wind angle (c).

Figure 25a shows the corresponding center of effort height measured oscillation, while Figures 25b-d show, respectively, the driving force, the heeling force, lift and drag measured time histories obtained from the experiment.

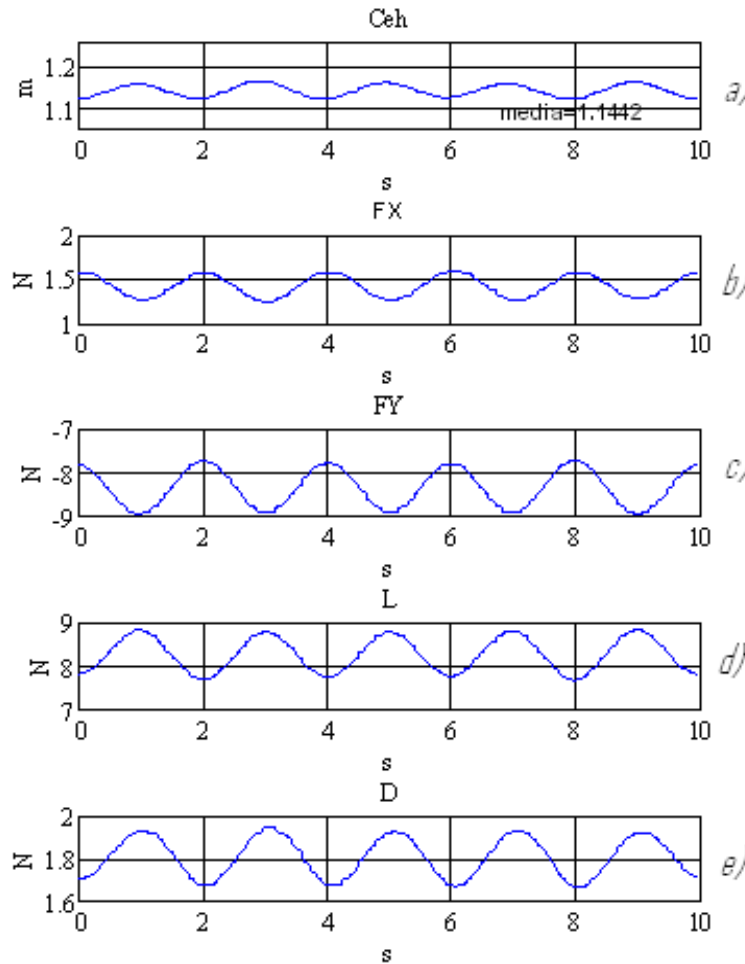


Figure 25. Sample of aerodynamic data obtained from forced motion dynamic wind tunnel tests.

These data were then further processed in order to represent the sail plan aerodynamic characteristics as described in the following.

RESULTS

In this section preliminary results obtained during dynamic wind tunnel tests are described. The scale model rig was tested in close-hauled conditions at apparent wind angle of 22° . The rig model was tested in upright conditions at constant wind tunnel speeds, subjected to harmonic pitch motion with different amplitudes and different frequencies.

A type of aerodynamic hysteresis loop resulted when the aerodynamic coefficients were plotted against the dynamic apparent wind angle β_{din} evaluated at the center of effort height during the rig model oscillation time period. For example, Figure 26 shows the measured aerodynamic driving force coefficient C_X and heeling force coefficient C_Y plotted against the dynamic apparent wind angle β_{din} .

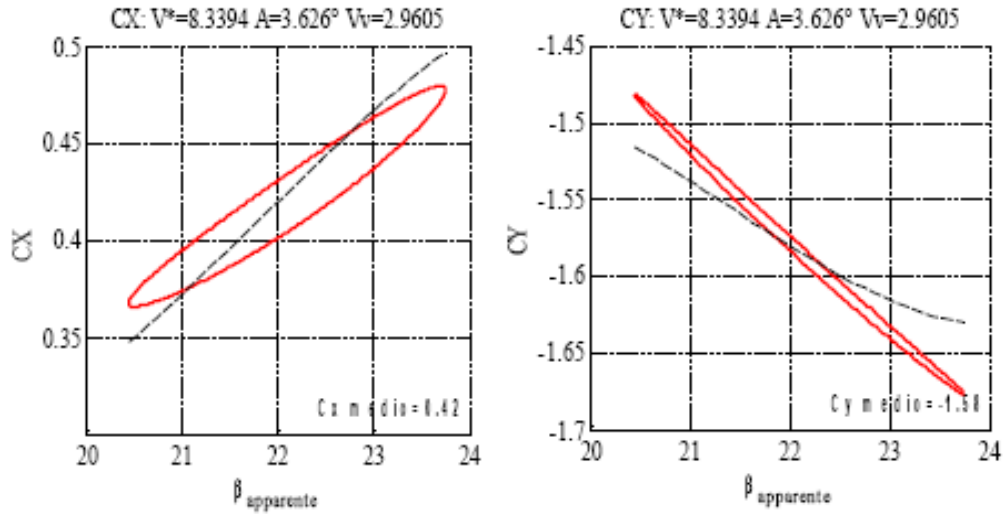


Figure 26. Driving and heeling dynamic force coefficients vs. β_{din} .

These results were obtained from a sinusoidal harmonic test where the rig model is driven with a pitch angle of 4° and a frequency of 0.5 Hz with a mean apparent wind speed of 3 m/s. The aerodynamic coefficients were calculated at each time step (i.e. at each dynamic apparent wind angle β_{din}) according to the following relationship:

$$C_X = \frac{F_X}{\frac{1}{2} \rho V_{ris}^2 S} \quad (15)$$

$$C_Y = \frac{F_Y}{\frac{1}{2} \rho V_{ris}^2 S}$$

where F_X and F_Y are the measured aerodynamic driving and heeling force components, respectively, S is the sail plan total area (main+jib), and V_{ris} is the dynamic resultant wind speed evaluated at the center of effort height.

In Figure 26, the steady-state coefficient curves previously obtained from traditional wind tunnel tests are shown as dashed lines. The steady-state curves relate to the sail trim that corresponds to the maximum driving force the sails can potentially achieve.

Figure 27 shows the corresponding lift and drag coefficients developed by the sails in dynamic conditions with the cyclical variation of the angle of attack resulting from the pitch oscillation. The coefficients were obtained from the lift and drag forces according to:

$$C_L = \frac{L}{\frac{1}{2} \rho V_{ris}^2 S} \quad (16)$$

$$C_D = \frac{D}{\frac{1}{2} \rho V_{ris}^2 S}$$

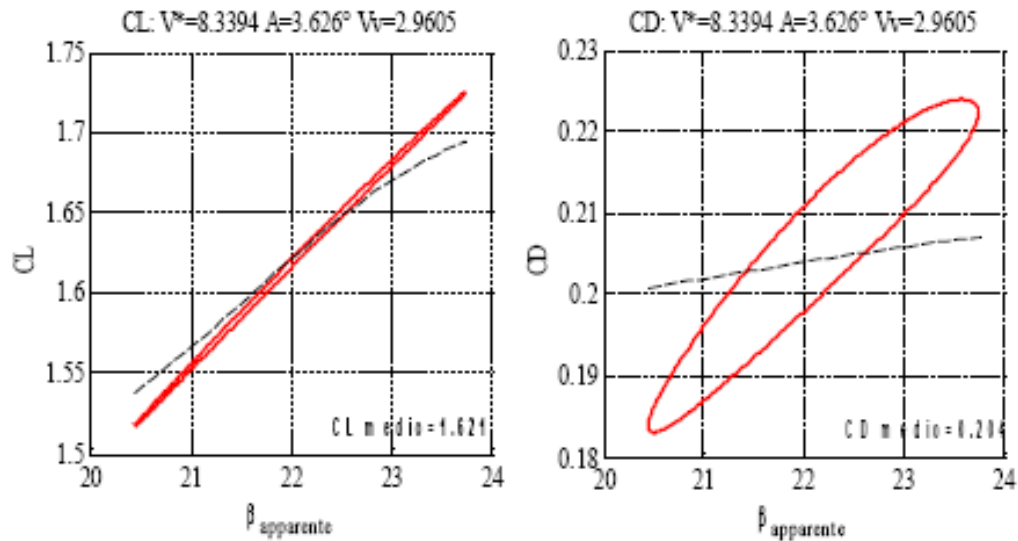


Figure 27. Lift and drag dynamic coefficients vs. $\beta_{din..}$

The driving and heeling force coefficients as well as lift and drag developed in dynamic conditions are different for a given angle of incidence (dynamic apparent wind angle) depending on whether that angle is increasing or decreasing. This leads to a hysteresis loop, which denotes the presence of a phase shift between the force and the instantaneous angle of attack $\beta_{din.}$ If the force and the instantaneous angle of attack were perfectly in phase, the hysteresis loop would appear as a single line equivalent to the static steady-state coefficient trend. When the force and the angle of attack are out of phase, the plot appears as a loop. The area inside the loop represents the amount of energy that can be dissipated or put into the system by the aerodynamic forces depending on the sign of the phase shift.

The loop axis has a different slope with respect to the steady-state curve slope. This means that dynamic effects influence both the equivalent damping and stiffness characteristics of the aerodynamic forces field.

Tests results have been organized in such a way as to compare aerodynamic forces obtained at a different reduced velocity corresponding to different imposed rig motion frequencies and mean wind speeds. A wide reduced velocity range (from 5 to more than 40) was investigated by changing the mean wind speed from 2 m/s to 4 m/s and the motion frequency from 0.1 Hz to 1.2 Hz.

Figures 28-30 show the lift coefficient developed by the sails in dynamic conditions with the cyclical variation of the angle of attack from several pairs of similar reduced velocity values obtained from different combinations of wind speed and pitch motion frequency:

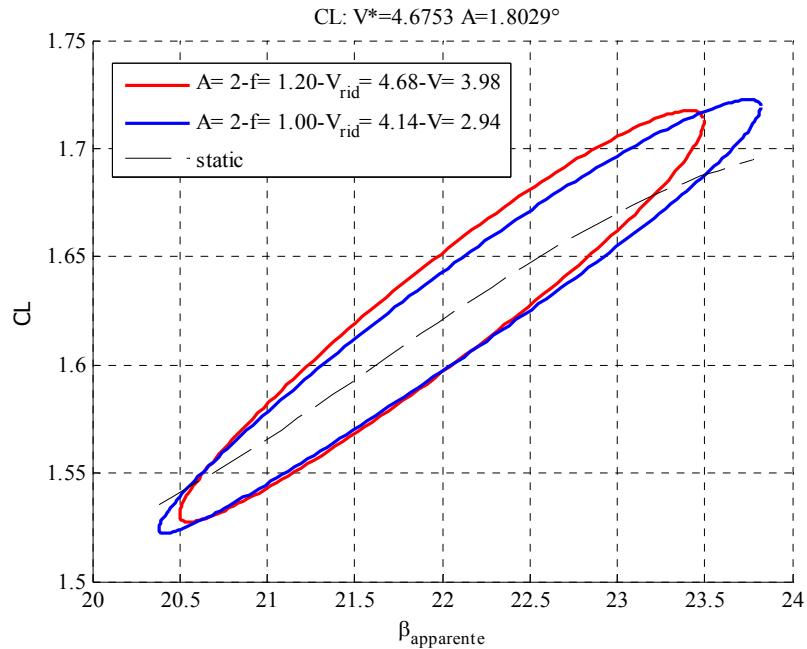


Figure 28. Lift dynamic coefficients vs. β_{din} at similar reduced velocities.

These results experimentally verify the fundamental nature of the reduced velocity as a way to define unsteady sail plan aerodynamics. Lift forces arising from different pairs of wind velocity and sail plan motion frequency at an equivalent reduced velocity basically overlay on the graph.

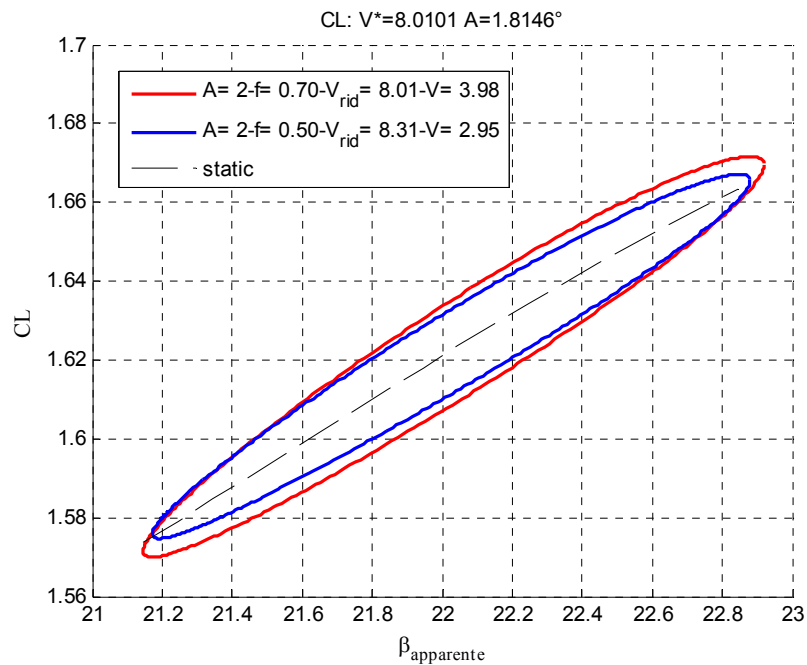


Figure 29. Lift dynamic coefficients vs. β_{din} at similar reduced velocities.

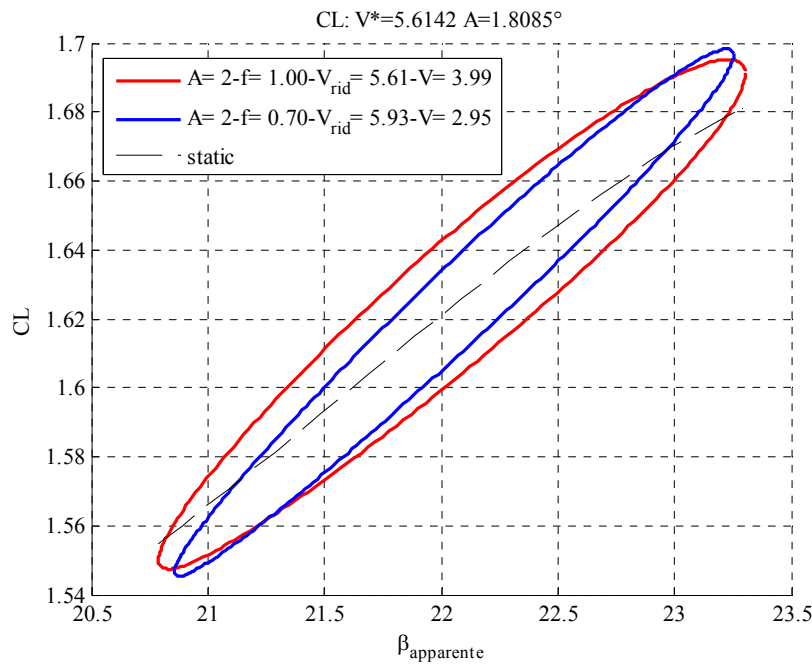


Figure 30. Lift dynamic coefficients vs. β_{din} at similar reduced velocities.

Figures 31 and 32 show the driving and heeling force coefficients at 3 m/s apparent wind speed with a medium pitch amplitude of 5° within the explored reduced velocity range (from $V_R = 5$ up to $V_R = 42$). Steady-state curves obtained from traditional wind tunnel tests are also shown. The fundamental role of reduced velocity in sail plan aerodynamics is once again demonstrated.

The increase of the hysteresis loop area, moving toward the lowest reduced velocity values (or towards the greatest reduced frequencies), corresponds to an increase in the aeroelastic damping effects at low V_R .

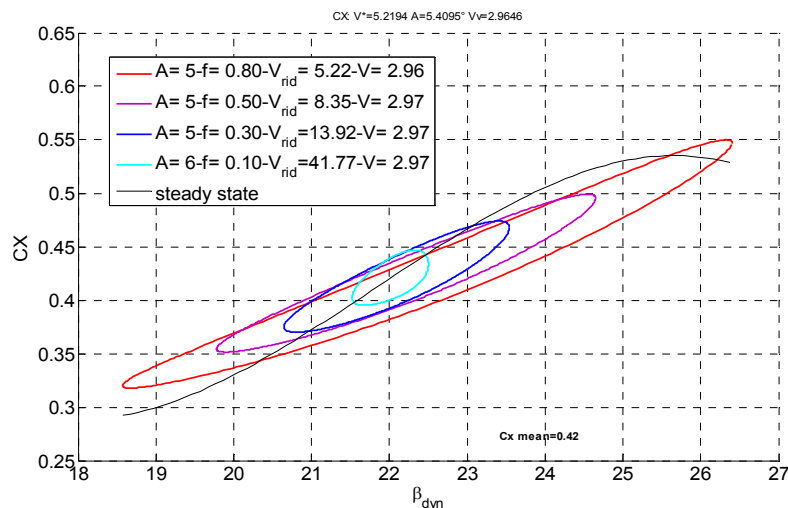


Figure 31. Driving force coefficient vs. β_{din} at different reduced velocities.

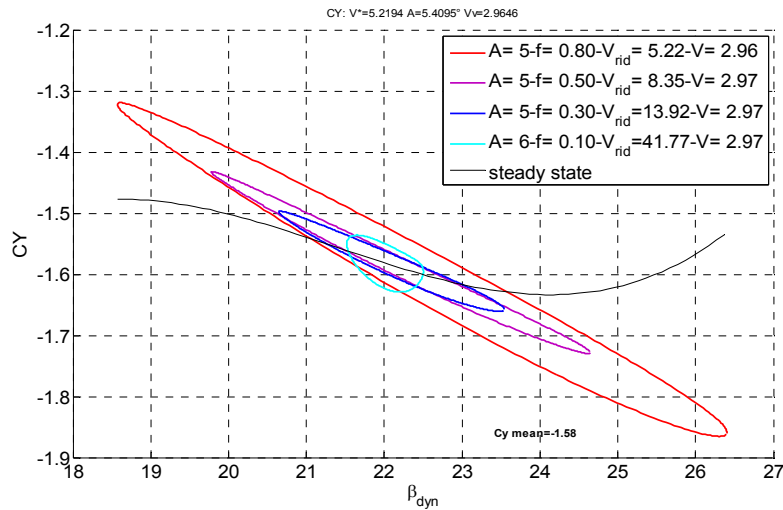


Figure 32. Heeling force coefficient vs. β_{din} at different reduced velocities.

The enclosed area of the hysteresis loop and the loop axis slope increase as the reduced velocity decreases, indicating that unsteady conditions lead to an aerodynamic equivalent damping effect and an equivalent stiffness variation.

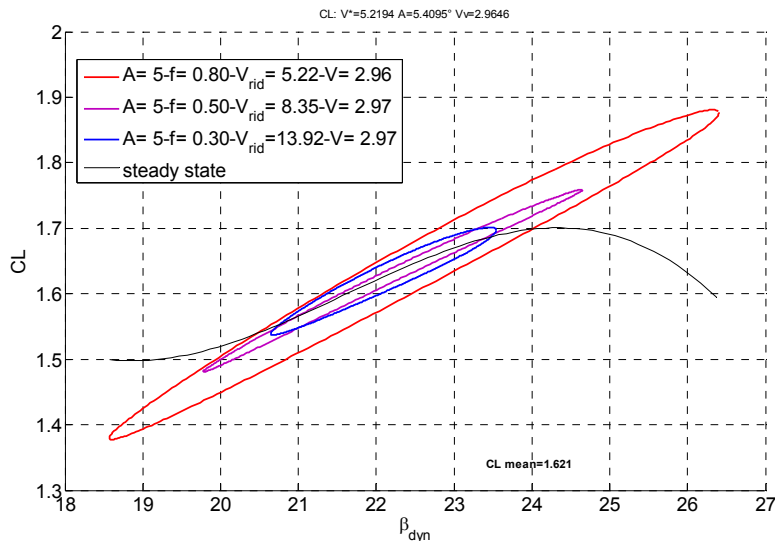


Figure 33. Lift coefficient vs. β_{din} at different reduced velocities.

Figures 33 and 34 show the difference between steady-state lift and drag coefficients and the corresponding unsteady aerodynamic coefficients within the same reduced velocity range.

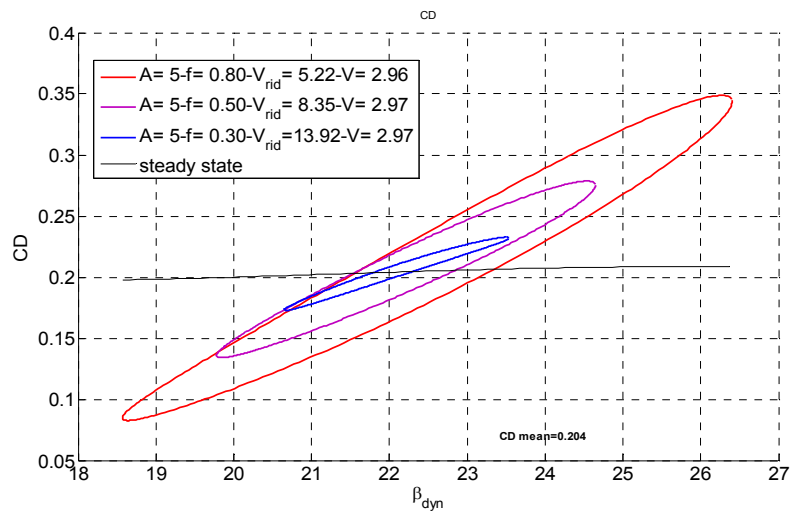


Figure 34. Drag coefficient vs. β_{din} at different reduced velocities.

From these figures we can conclude that drag- and lift-associated stiffening and damping equivalent effects increase with unsteady conditions.

The cycles move around the mean static coefficient curve with the apparent wind angle. Increasing the pitch frequency leads to a wider instantaneous apparent wind angle (i.e., dynamic angle of attack) range near the mean apparent wind angle value that represents the steady-state reference condition.

Figures 35 and 36 refer to tests with a smaller pitch amplitude of 2° performed at a higher apparent wind tunnel speed (4 m/s) within a reduced velocity range of 5.61-28.

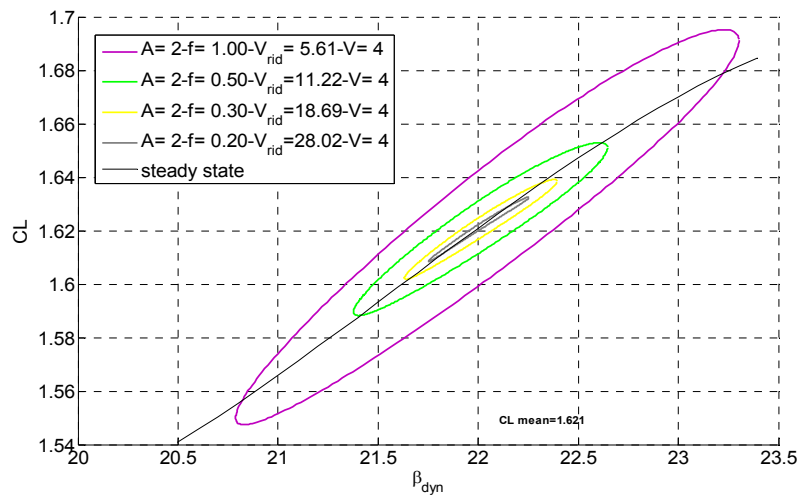


Figure 35. Lift coefficient vs. β_{din} at different reduced velocities.

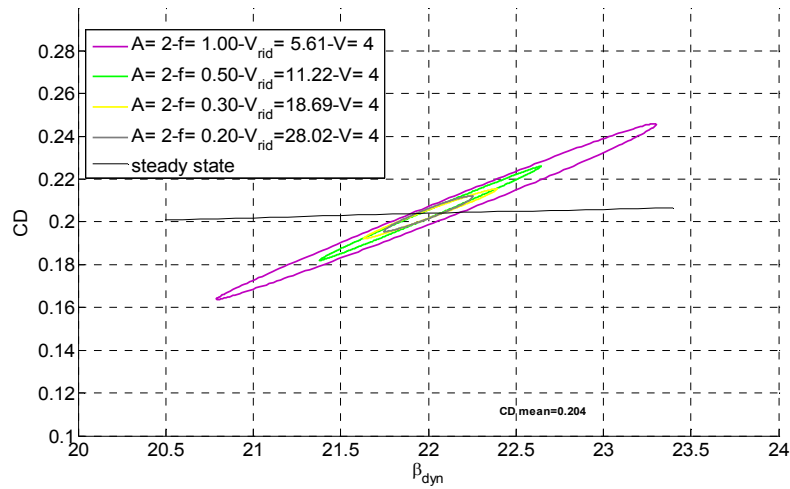


Figure 36. Drag coefficient vs. β_{din} at different reduced velocities.

Figures 37 and 38 refer to tests performed at 3 m/s apparent wind speed with a pitch amplitude of 2° and within a reduced velocity range of 3.46-14.

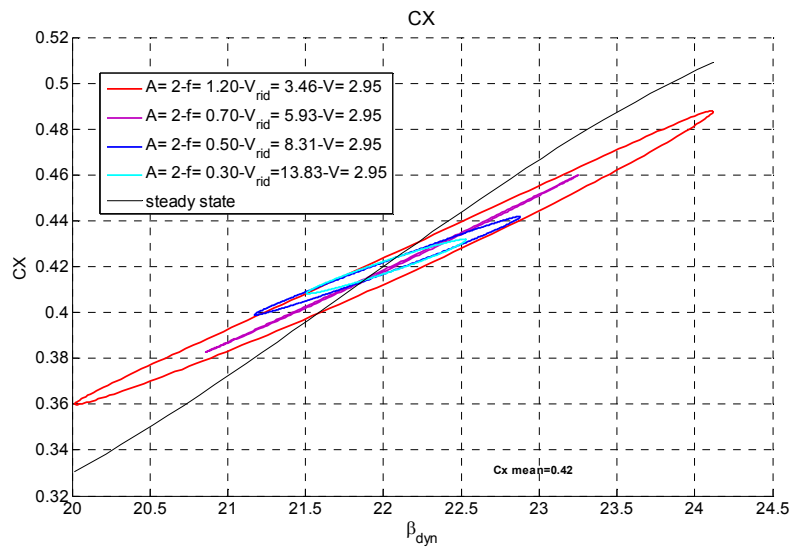


Figure 37. Driving force coefficient vs. β_{din} at different reduced velocities.

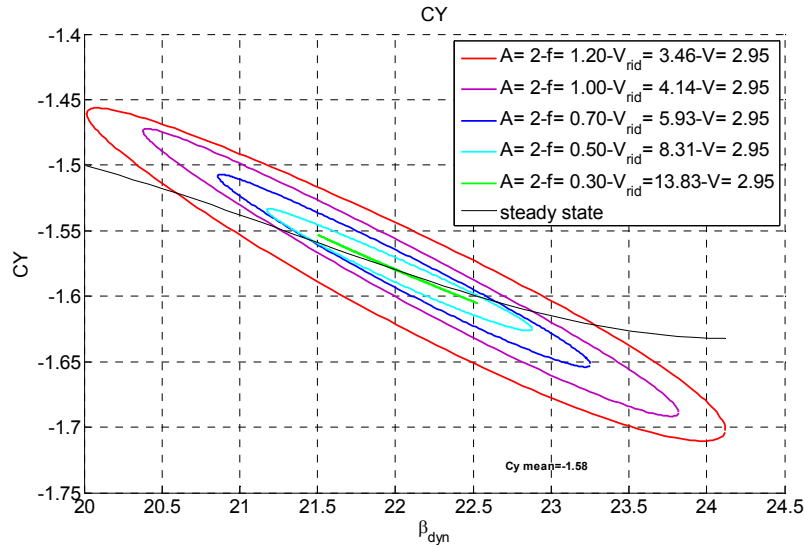


Figure 38. Heeling force coefficient vs. β_{din} at different reduced velocities.

Figures 39 and 40 show the heeling and driving force coefficients obtained at the same reduced velocity with pitch oscillation amplitudes ranging from 2° to 9° .

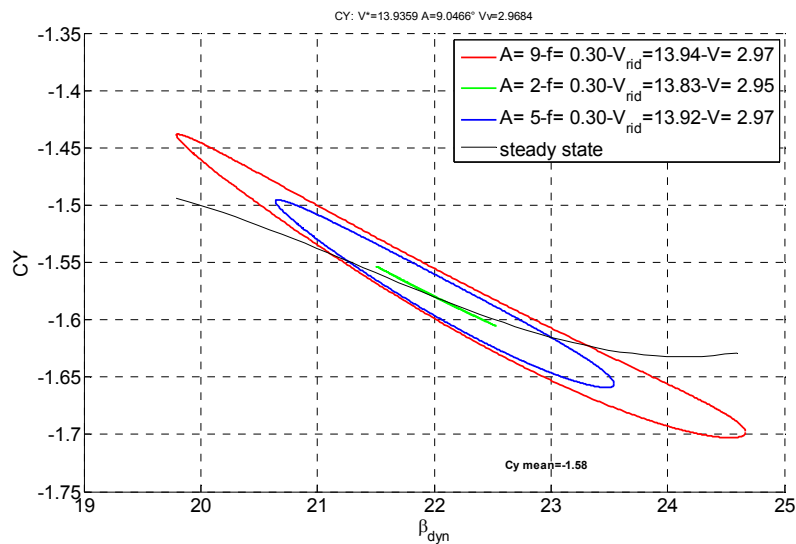


Figure 39. Heeling force coefficient vs. β_{din} at the same reduced velocity with different pitch amplitudes.

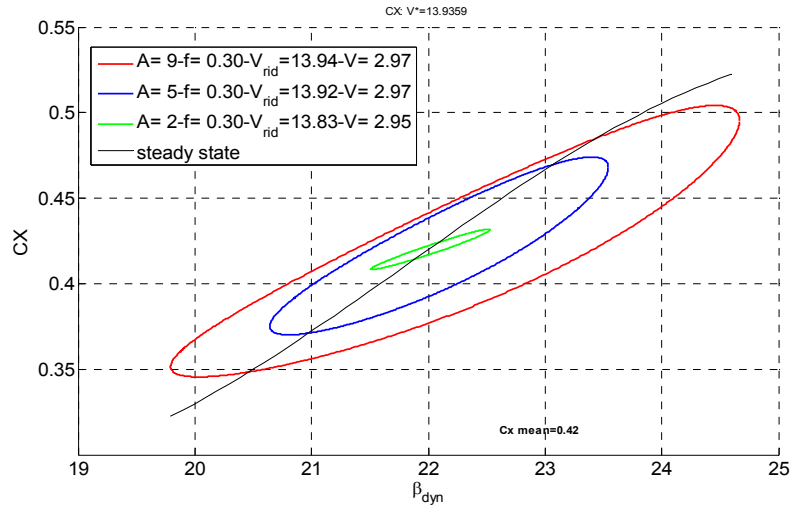


Figure 40. Driving force coefficient vs. β_{din} at the same reduced velocity with different pitch amplitudes.

The deformed hysteresis loop indicates a non-linear dependence on the angle of attack according to the static coefficient trend. The aerodynamic behavior is more linear at smaller pitch amplitudes. The loops are not perfectly elliptical at larger pitch angles and are a function of the level of amplitude of the angle of attack due to the rig motion.

Figures 41 and 42 show the corresponding lift and drag coefficients.

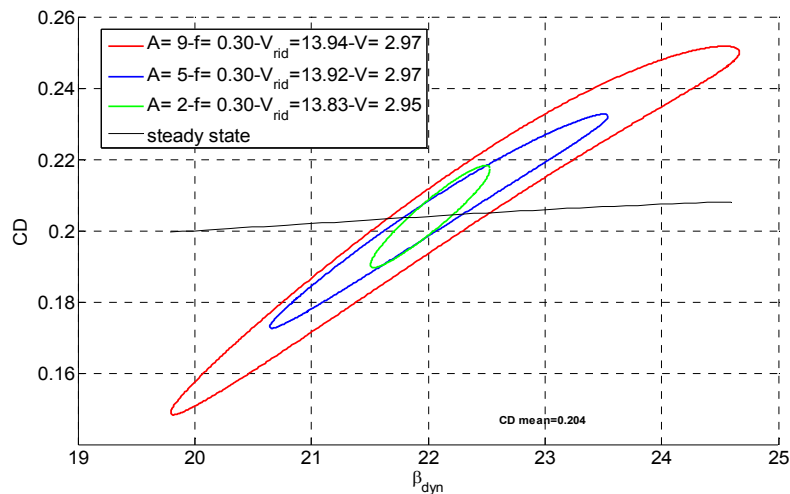


Figure 41. Drag coefficient vs. β_{din} at the same reduced velocity with different pitch amplitudes.

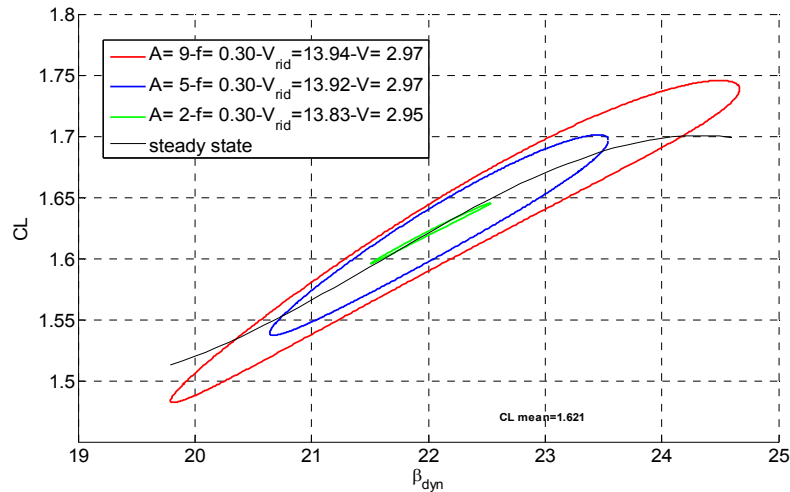


Figure 42. Lift coefficient vs. β_{din} at the same reduced velocity with different pitch amplitude.

Figure 43 shows the effect of pitch amplitude on the driving force coefficient at higher reduced velocity.

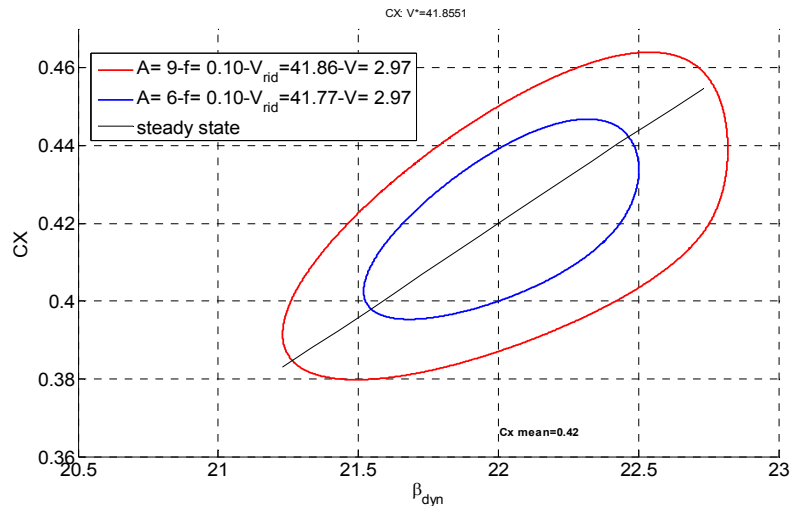


Figure 43. Driving force coefficient vs. β_{din} at the same reduced velocity with different pitch amplitudes.

ON THE ADDED MASS EFFECTS

To account for inertia, “wind-off” tests were performed for each chosen frequency and pitch amplitude combination. The differences between “wind-on” and “wind-off” measurements were then used to evaluate the aerodynamic forces developed by the sail plan in dynamic conditions.

The aerodynamic inertia resulting from the added mass of the sails is generally used to characterize the change in kinetic energy of air around the sails caused by changes in the yacht's linear or angular velocity.

In order to quantify the added inertia of the sails, the time histories of the measured pitch moment during the "wind-off" tests were compared with the calculated pitch moment of inertia using the mechanical model of the experimental test rig.

The experimental setup was modeled using the CATIA multi-body software analysis tool. The moment of inertia in pitch was calculated considering the actual geometric layout of the scale model yacht rig, the dynamometric balance, and the weighted part of the pitching device using the material and mass density properties of each component.

Figure 44 shows an example of the CATIA model with reference to the mainsail-only test case.

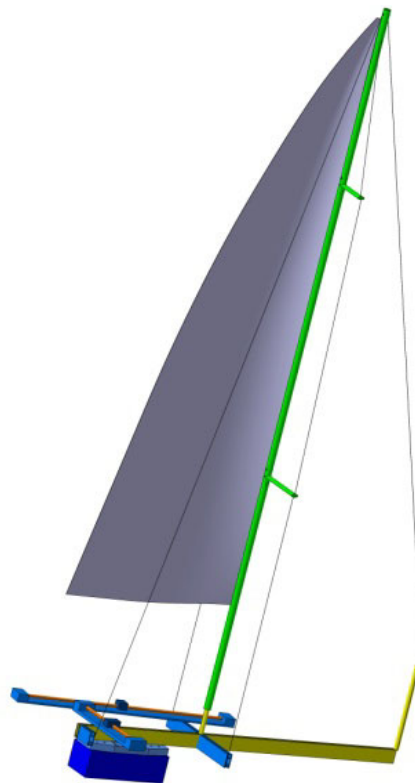


Figure 44. Experimental setup multi-body model.

Using this model, the mass moment of inertia relative to the pitch axis of the experimental system including the rig and the sails was calculated to be:

$$I = 3.734 \text{ kg} \cdot \text{m}^2 \quad (17)$$

Then the harmonic transfer function between the measured pitch moment in the "wind-off" tests and the pitch acceleration imposed by the computer-controlled servo-hydraulic actuator at the various pitch amplitudes and frequencies considered during the rig forced motion tests was evaluated. This transfer function is shown in Figure 45:

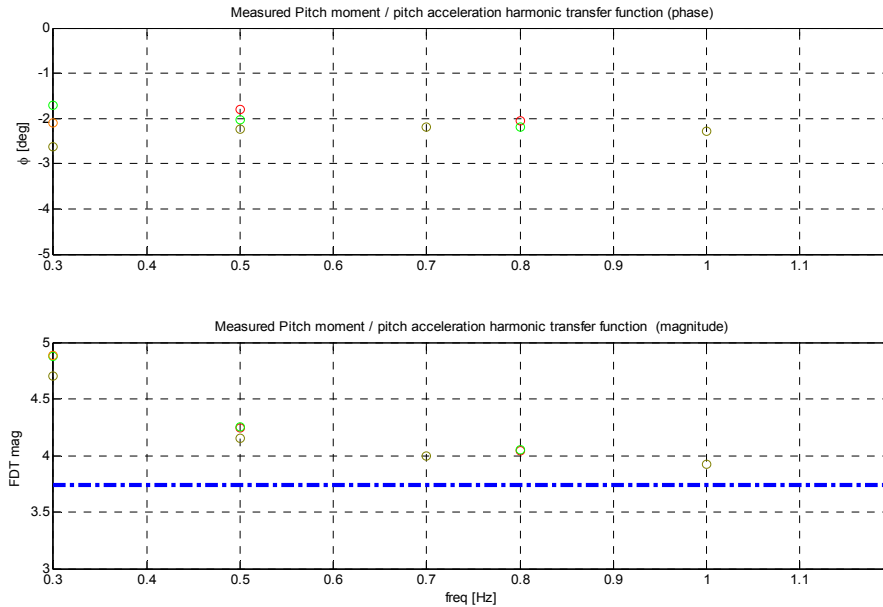


Figure 45. Measured harmonic transfer function between the pitch moment and the pitch acceleration.

The pitch moment measured in the "wind-off" condition is usually in phase with the measured sail plan pitch acceleration with a phase shift of 2° to 3°. This means the measured force of the pitch motion in still air is directly proportional to the acceleration.

The harmonic transfer function magnitude represents the total inertia of the system I^* which can be considered as the superposition of the mass moment of inertia of the system (I) and the added moment of inertia J_{added} which we want to evaluate:

$$I^* = I + J_{added} \tag{18}$$

Figure 45 shows the measured total inertia of the system I^* versus frequencies considered during the "wind off" forced motion test. The blue dotted line represents the calculated mass moment of inertia of the system (I).

The order of magnitude of the added moment of inertia J_{added} asymptotically approaches about 10% of the system mass moment of inertia with an increasing trend at the lower frequencies. However, during our tests, the inertia of the system was 10 times larger than the J_{added} that was to be measured, so the accuracy of the measured values at frequencies lower than 0.3 Hz is poor due to the very low values to be measured. More accurate

results in the low frequency range might be obtained using a smaller dynamometric balance with a lower measuring range.

CONCLUSIONS

Dynamic effects on sail plan aerodynamics due to yacht motion induced by sea waves were investigated by means of wind tunnel tests performed in dynamic conditions. In particular a rigid carbon fiber scale model rig of a 48' cruiser-racer was tested in close-hauled conditions at an apparent wind angle of 22°.

Yacht pitch frequency and amplitude effects were analyzed.

A "sail plan reduced velocity" concept was defined using the sail plan center of effort as a reference point, and a fundamental role of this "sail plan reduced velocity" was highlighted.

The concepts of a generalized "instantaneous apparent wind angle" (dynamic apparent wind angle) and a generalized "instantaneous apparent wind speed" (dynamic apparent wind speed) were introduced in order to manage the 3D mainsail and jib aerodynamics.

Preliminary results were obtained by investigating a wide range of reduced velocities (from 5 to more than 40) and the dependence on the angle of attack.

A new representation of the aeroelastic effects was proposed in the form of aerodynamic hysteresis loops which were obtained by plotting the aerodynamic coefficients against the instantaneous apparent wind angle, and varied using a harmonic law combining constant wind tunnel speed with the velocity at the sail plan center of effort induced by yacht pitch motion.

Preliminary results show that that reduced velocity plays a fundamental role in sail plan aerodynamics. As the reduced velocity decreases, the enclosed area of the hysteretic loop and the loop axis slope increase. This means that unsteady conditions lead to aerodynamic equivalent damping and stiffening effects.

By increasing the instantaneous apparent wind angle variations, the aerodynamic coefficients hysteresis loop is deformed according to the static coefficients trend. This denotes non-linear dependence on the angle of attack.

These preliminary results represent the first step in research into this topic, aimed at investigating sail plan aerodynamics in unsteady conditions. Based on these results, the following additional developments are currently in progress:

- a deeper experimental investigation of the aerodynamic hysteresis loop with a wider range of apparent wind angles
- the addition of sail plan roll motion induced by sea waves
- a numerical investigation to determine suitable analytical or numerical models capable of reproducing sail plan unsteady aerodynamics

The final stage of the research should be to include the previously mentioned numerical model into a dynamic VPP in the time domain, thus allowing for the analysis of sailing yacht behavior in a realistic environment.

Acknowledgements

The authors wish to thank Prof. Keuning of Delft University of Technology, who provided the heave and pitch Response Amplitude Operator (RAO) for model 455 from the DSYHS.

REFERENCES

- Caracoglia, L., and Jones, N.P. (2003). "Time domain vs. frequency domain characterization of aeroelastic forces on bridge deck sections." *Journal of Wind Engineering and Industrial Aerodynamics*, 91, 371-401.
- Cloughton, A.R., Shenoi, R.A., and Wellicome, J.F. (1998). *Sailing yacht design: Theory*. Addison Wesley Longman.
- Contento, G., Ledri, M., and Codiglia, L. (2006). "Experimental analysis of the vertical motions in waves of an IACC yacht with calm water-optimized bulb shapes." *Proceedings of the 2nd High Performance Yacht Design Conference*, Auckland, 82-88.
- Dickinson, M.H., and Goetz, K.G. (1993). "Unsteady aerodynamic performance of model wings at low Reynolds numbers." *Journal of Experimental Biology*. 174, 45-64.
- Fossati, F., Cloughton, A., Battistin, D., and Muggiasca, S. (2008). "Changes and development to sail aerodynamics in the ORC international rule." *Proceedings of the 20th HISWA Symposium*, Amsterdam.
- Fossati, F., Muggiasca, S., Zasso A., Viola I., (2006). "Wind tunnel techniques for investigation and optimization of sailing yachts aerodynamics." *Proceedings of the 2nd High Performance Yacht Design Conference*, Auckland.
- Fossati, F., Martina, F., and Muggiasca, S. (2008). "Experimental database of sail performance and flying shapes in upwind conditions." *Proceedings of the International Conference on Innovations in High Performance Sailing Yachts*, Lorient.
- Fossati, F. and Muggiasca, S. (2009). "Sails aerodynamic behavior in dynamic conditions." *Proceedings of the 19th Chesapeake Sailing Yacht Symposium*, Annapolis.
- Fung, Y.C. (1955). *An Introduction to the Theory of Aeroelasticity*. Wiley
- Gerhardt, F., Flay, R., and Richards, P. (2008). "Unsteady aerodynamic phenomena associated with sailing upwind in waves." *Proceedings of the 3rd High Performance Yacht Design Conference*, Auckland.
- Glauert, H. (1948). *The Elements of Airfoil and Airscrew Theory*. Cambridge University Press
- Hansen, H., Richards, P., and Jackson, P.S. (2006). "An investigation of aerodynamic force modelling for yacht sails using wind tunnel." *Proceedings of the 2nd High Performance Yacht Design Conference*, Auckland.
- Harris, D.H. (2002). "Simulation of upwind manoeuvring of a sailing yacht." PhD dissertation, University of Maryland, College Park.
- Kerwin, J.E. (1978). "A velocity prediction program for ocean racing yachts." Report No. 78-11, MIT.
- Keuning, J.A., Vermeulen, K.J., and de Ridder, E.J. (2007). "A generic mathematical model for the maneuvering and tacking of a sailing yacht." *Proceedings of the 18th Chesapeake Sailing Yacht Symposium*, Annapolis.
- Jackson, P.S. (2001). "An improved upwind sail model for VPP's." *Proceedings of the 15th Chesapeake Sailing Yacht Symposium*, Annapolis.
- Jain A., Jones, N.P., and Scanlan R.H. (1996). "Coupled aeroelastic response of long span bridges." *Journal of Wind Engineering and Industrial Aerodynamics*, 60, 69-80.

Lee, T., and Gerontakos, P. (2004). "Investigation of flow over an oscillating airfoil." *Journal of Fluid Mechanics*, 512, 313-341.

Masuyama, Y. (1997). "Full scale measurements of sail forces and the validation of the numerical calculation methods." *Proceedings of the 13th Chesapeake Sailing Yacht Symposium*, Annapolis.

Masuyama Y. et al. (1993). "Dynamic performance of sailing cruiser by full scale sea tests." *Proceedings of the 11th Chesapeake Sailing Yacht Symposium*, Annapolis.

Masuyama, Y., et al. (1995). "Tacking simulation of a sailing yacht." *Proceedings of the 12th Chesapeake Sailing Yacht Symposium*, Annapolis.

Milgram, J. (1971). "Section data for thin highly cambered airfoils in incompressible flow." NASA CR-1767.

Molyneux, W.G. (1956). "Measurement of the aerodynamic forces on oscillating airfoils." AGARD Rep. 35.

Moss, G.F., and Murdin, P.M. (1971). "Two-dimensional low speed tunnel tests on the NACA 0012 section including measurements made during pitch oscillations at the stall." *Aeronautical Research Council, ARC C.P. No 1145*.

Richardt, T., Harries, S., and Hochkirch, K. (2005). "Maneuvering simulations for ships and sailing yachts using FRIENDSHIP equilibrium as an open modular workbench." *International EuroConference on Computer Applications and Information Technology in the Maritime Industries (COMPIT)*, Hamburg.

Schlichting, H., and Truckenbrodt, E. (1979). *Aerodynamics of the Airplane*. McGraw-Hill.

Theodorsen, T. (1949). "General theory of aerodynamic instability and the mechanism of flutter." NACA TR-496.